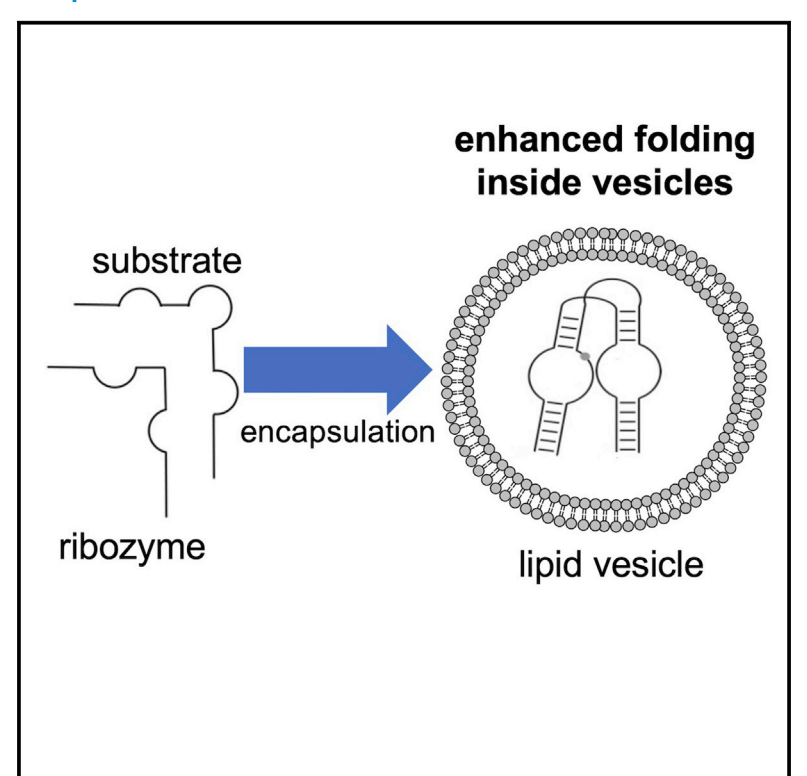
# Vesicle encapsulation stabilizes intermolecular association and structure formation of functional RNA and DNA

# **Graphical abstract**



# **Authors**

Huan Peng, Amandine Lelievre, Katharina Landenfeld, Sabine Müller, Irene A. Chen

# Correspondence

ireneachen@ucla.edu

# In brief

Peng et al. study the effect of vesicle encapsulation on the hairpin ribozyme, a stem-loop RNA, and a pH-sensitive DNA switch. They find that encapsulation enhances RNA association and tertiary folding of the nucleic acids. These effects could promote the emergence of biological functions in an RNA world of early life.

# **Highlights**

- Encapsulation enhances the cleavage and ligation activities of hairpin ribozymes
- Encapsulation promotes RNA-RNA association and DNA triplex structures
- Encapsulation rescues the activity of folding-deficient hairpin ribozyme mutants









# **Article**

# Vesicle encapsulation stabilizes intermolecular association and structure formation of functional RNA and DNA

Huan Peng, 1 Amandine Lelievre, 2 Katharina Landenfeld, 2 Sabine Müller, 2 and Irene A. Chen 1,3,\*

- <sup>1</sup>Department of Chemical and Biomolecular Engineering, University of California, Los Angeles, Los Angeles, CA 90095, USA
- <sup>2</sup>Institute of Biochemistry, University of Greifswald, 17487 Greifswald, Germany

\*Correspondence: ireneachen@ucla.edu https://doi.org/10.1016/j.cub.2021.10.047

# **SUMMARY**

During the origin of life, encapsulation of RNA inside vesicles is believed to have been a defining feature of the earliest cells (protocells). The confined biophysical environment provided by membrane encapsulation differs from that of bulk solution and has been shown to increase activity as well as evolutionary rate for functional RNA. However, the structural basis of the effect on RNA has not been clear. Here, we studied how encapsulation of the hairpin ribozyme inside model protocells affects ribozyme kinetics, ribozyme folding into the active conformation, and cleavage and ligation activities. We further examined the effect of encapsulation on the folding of a stem-loop RNA structure and on the formation of a triplex structure in a pH-sensitive DNA switch. The results indicate that encapsulation promotes RNA-RNA association, both intermolecular and intramolecular, and also stabilizes tertiary folding, including the docked conformation characteristic of the active hairpin ribozyme and the triplex structure. The effects of encapsulation were sufficient to rescue the activity of folding-deficient mutants of the hairpin ribozyme. Stabilization of multiple modes of nucleic acid folding and interaction thus enhanced the activity of encapsulated nucleic acids. Increased association between RNA molecules may facilitate the formation of more complex structures and cooperative interactions. These effects could promote the emergence of biological functions in an "RNA world" and may have utility in the construction of minimal synthetic cells.

# INTRODUCTION

The encapsulation of nucleic acids, particularly RNA, is a subject of increasing interest in bottom-up synthetic biology. Ribozymes encapsulated inside simple vesicles are an important experimental model of the "RNA world" of early cells, as encapsulation is essential for creating the physical and genetic units of the cell. 1-7 In addition, vesicles encapsulating gene circuits are a potential platform for artificial cells.8-11 Interactions between RNA and vesicles can result in a rich range of emergent behaviors, including vesicle growth driven osmotically by RNA, 12 control of ribozyme reactions by oligonucleotides during vesicle growth, 13 and physical stabilization of fatty acid vesicles by nucleobases. 14 Encapsulation itself has been observed to increase the binding activity of an RNA aptamer<sup>15</sup> and to accelerate evolutionary adaptation<sup>16</sup> during in vitro selection of ribozymes by increasing the variance of fitness. However, the structural basis for these changes in activity and fitness is not well understood.

RNA function depends on structure, <sup>17</sup> which is critically influenced by the chemical and biophysical environment. The cellular environment is understood to have important effects in modern cells through chemical interactions as well as excluded volume effects. Molecular crowding has been shown to improve the

activity of the hairpin ribozyme by increasing the rate of docking, 18 increase the activity of a hepatitis delta virus (HDV)-like ribozyme under relatively low Mg<sup>2+</sup> concentrations, <sup>19</sup> increase the activity of the hammerhead ribozyme, 20,21 and increase the activity of a group I ribozyme, compensating for low Mg<sup>2+</sup> concentrations.<sup>22</sup> Molecular crowding agents appear to stabilize compact folds, as demonstrated for a group II intron ribozyme<sup>23</sup> and a group I ribozyme, 24,25 to the extent that molecular crowding rescues the activity of group I ribozyme mutants.<sup>26</sup> Similarly, the activity of a bimolecular version of RNase P ribozymes is improved by crowding agents, as constructs with no detectable activity can be activated by addition of polyethylene glycol.<sup>27</sup> In an aqueous two-phase system, the partitioning of RNA creates a concentrated and crowded phase in which ribozyme activity is substantially enhanced.<sup>28</sup> Confinement of a macromolecule inside a membrane vesicle creates an excluded volume effect similar to crowding. On theoretical grounds, like crowding, encapsulation is predicted to favor compact structures, shifting the conformational equilibrium toward folded, functional structures.29

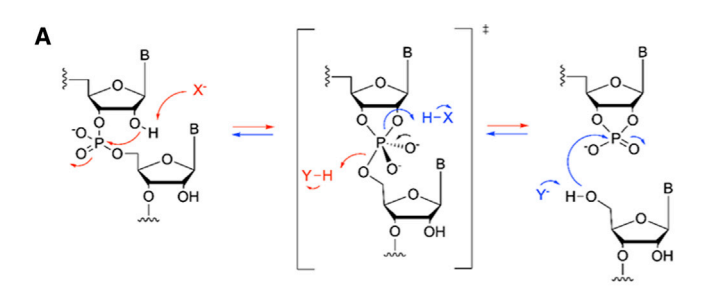
Here, we probed the effect of encapsulation on nucleic acid association, structure, and function, using three model systems: the hairpin ribozyme, an RNA stem loop, and a pH-sensitive DNA switch. The hairpin ribozyme is a small self-cleaving

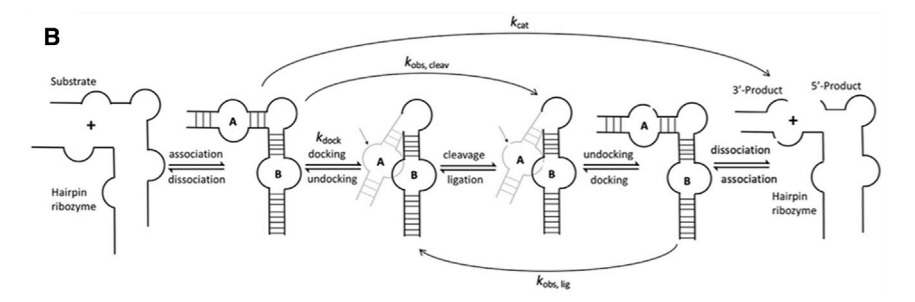


<sup>3</sup>Lead contact

# **Article**







ribozyme derived from the tobacco ringspot virus satellite RNA,30,31 whose mechanism and folding pathway is well studied (Figure 1A). The naturally self-cleaving hairpin ribozyme structure can be engineered for cleavage in trans, such that suitable RNA substrates are cleaved in a multiple-turnover reaction. Cleavage is reversible, and both cleavage and ligation reactions proceed via the same reaction path in opposite directions.<sup>32</sup> The minimal catalytic structure of the hairpin ribozyme consists of four Watson-Crick base-paired helices separated by two loops (A and B). A key element of the catalytic complex is a "docked" intermediate, in which loops A and B are brought into close contact. 33,34 Upon docking, the catalytic center is created and a transesterification reaction occurs, in which the O2' at the cleavage site attacks the adjacent phosphodiester linkage by an S<sub>N</sub>2-like mechanism, with departure of the O5' and formation of a cyclic 2',3'-phosphate (Figure 1).35 A stably docked intermediate is essential for ligation activity, but selfcleavage can occur, albeit at a reduced rate, even for mutants in which the ribozyme is only transiently docked. 36,37 Therefore, formation of the docked intermediate affects reactivity. Docking has been monitored in fluorescence resonance energy transfer (FRET) assays by labeling the two stems with appropriate donor and acceptor dyes. 33,38,39 When conducted in trans under multiple-turnover conditions, the hairpin ribozyme reaction follows Michaelis-Menten kinetics, allowing the effect of lipids and encapsulation to be separately evaluated for catalytic steps or substrate association. To probe the effect of encapsulation on secondary structure formation alone, an RNA stem loop was used as a simple two-state folding system. Then, to probe how encapsulation affects the formation of noncanonical base pairing, intramolecular triplex formation in a DNA "switch" was studied.

Vesicles made from fatty acids are a model for primitive or artificial cells, as they allow for the diffusion of nutrients and ions and exhibit a variety of dynamic behaviors on a laboratory timescale, including sustainable growth and division cycles coupled with encapsulated RNA replication. 40–43 Although fatty acid vesicles

# Figure 1. Catalysis by the hairpin ribozyme

(A) Reaction mechanism of the hairpin ribozyme (red: cleavage; blue: ligation).

(B) Folding pathway of the hairpin ribozyme (adapted from Zhuang et al.  $^{34}$ ). Measured parameters correspond to steps as indicated. Note that  $k_{\rm obs,cleav}$  includes the docking and cleavage steps.

are very sensitive to the presence of divalent cations, the addition of phospholipids to these vesicles results in greater stability, enabling the study of ribozymes that have relatively high Mg<sup>2+</sup> requirements. 44 While lipids may exhibit effects on RNA due to chemical interactions in addition to excluded volume effects, the comparison of encapsulated RNA to non-encapsulated RNA, exposed to empty vesicles, controls for chemical interactions and can thereby isolate the effect of confinement. 15 We find that encapsulation stabi-

lizes multiple modes of nucleic acid folding, including intermolecular RNA-RNA association, secondary structure formation, and tertiary interactions.

# **RESULTS**

# Multiple-turnover kinetics of the hairpin ribozyme: encapsulation preserves and enhances cleavage activity

Vesicles were prepared from a 1:1 mixture of oleic acid and POPC (1-palmitoyl-2-oleoyl-glycero-3-phosphocholine), composition known to be stable in the presence of 10 mM Mg<sup>2+</sup>.<sup>44</sup> Large unilamellar vesicles were prepared by extrusion to 100 nm diameter (Figure S1A). We determined the cleavage activity of the hairpin ribozyme in the absence of vesicles (i.e., in buffer without lipids), exposed to empty vesicles but not encapsulated ("OutV") and encapsulated inside vesicles ("InV"). Since the activity of the hairpin ribozyme is dependent on Mg<sup>2+</sup> concentration, [Mg<sup>2+</sup>] was varied from 5 to 10 mM. The lipid concentration was varied from 10 to 50 mM to test the dependence of activity on [lipid]. To determine Michaelis-Menten rate constants in a multiple-turnover reaction with excess substrate, the ribozyme:substrate ratio was varied from 1:5 to 1:100.

We determined the Michaelis constant ( $K_{\rm m}$ ) and catalytic rate constant ( $k_{\rm cat}$ ) of the hairpin ribozyme under the different conditions. Cleavage of substrate RNA 1 (Table S1) by the ribozyme releases a 6-nucleotide, dye-labeled product (Figure 2A). Product formation was followed over time by denaturing gel electrophoresis (Figure 3) and fit to a Michaelis-Menten kinetic model following a previously described procedure (Figures S1–S3; STAR Methods). <sup>45</sup>

 $K_{\rm m}$  and  $k_{\rm cat}$  for encapsulated ribozymes (InV) were compared to the values for ribozymes that were exposed to empty vesicles (OutV) or in lipid-free solution. Exposure to empty vesicles (i.e., having ribozymes on the outside of vesicles) caused increased  $K_{\rm m}$  (Figures 4A–4C), which is consistent with prior



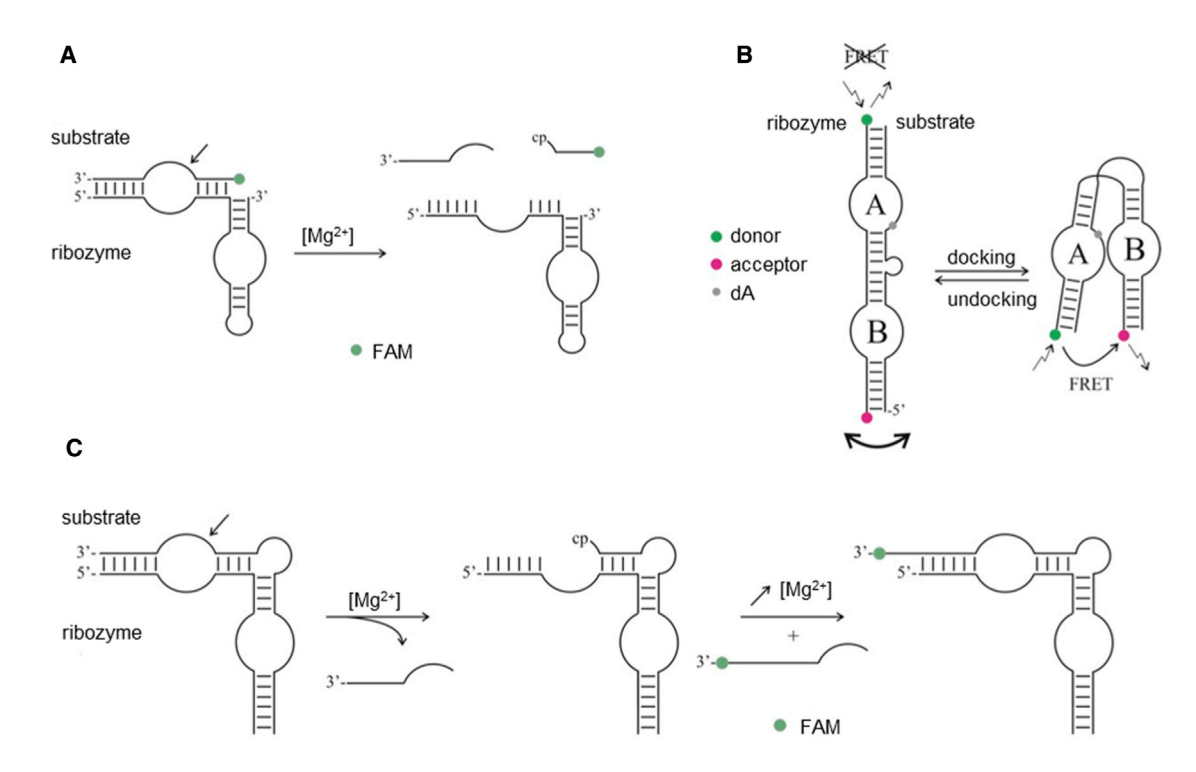


Figure 2. Assays of hairpin ribozyme activity and folding

(A) Cleavage of a fluorescently labeled substrate releases a fluorescent product that can be quantified by gel electrophoresis.

(B) Adoption of the docked conformation brings a FRET pair into close proximity, generating a signal. Adenosine at the cleavage site in loop A was replaced by its deoxy analog (dA) to prevent cleavage.

(C) In general, ligation-competent ribozyme-substrate complex is prepared by annealing the ribozyme strand with a cleavage substrate and conducting the cleavage reaction at 7 mM Mg<sup>2+</sup>. Dissociation of the smaller 3' cleavage product results in the ribozyme strand in complex with the 5' ligation substrate strand carrying the required 2',3'- cyclic phosphate (labeled "cp"). Then, the addition of a fluorescently labeled 3' substrate strand and higher [Mg<sup>2+</sup>] allows assessment of ligation activity by gel electrophoresis.

observations that lipids act as a denaturant. 46 Exposure to high concentrations of lipid caused a loss of detectable activity in the OutV condition (Figure S4). However, InV yields lower  $K_{\rm m}$ at the same lipid concentrations and preserved activity at concentrations that had resulted in no detectable activity in the OutV condition. In addition, at low [Mg<sup>2+</sup>] (5 mM; Figure 4A), encapsulation resulted in a significantly lower  $K_{\rm m}$  compared to the lipid-free solution, indicating that encapsulation can not only prevent loss of binding but also improve activity. While increasing lipid concentration caused increased  $K_{\rm m}$  in the OutV condition, InV rendered the  $K_{\rm m}$  insensitive to lipid concentration over the tested range.

A similar pattern was observed for the rate constant  $k_{cat}$  and catalytic efficiency  $k_{cat}/K_{m}$  (Figures 4D–4I, respectively). Exposure to increasing lipid concentration (OutV) decreased  $k_{cat}$ and  $k_{\text{cat}}/K_{\text{m}}$ , with activity being undetectable at high lipid concentrations (Figure S4I), again, consistent with denaturation upon lipid exposure. However, when InV,  $k_{cat}$  and  $k_{cat}/K_{m}$ remained high and were not affected by lipid concentration, tolerating lipid concentrations that would otherwise result in no activity (STAR Methods).

Notably, encapsulation was observed to prevent inactivation of the hairpin ribozyme at higher lipid concentrations (Figure 4). At low [Mg<sup>2+</sup>] (5 mM), exposure to empty vesicles with  $\geq$ 30 mM lipid caused inactivation of the ribozyme (i.e., undetectable activity in the OutV condition), but encapsulated ribozymes were active at all of the lipid concentrations tested (STAR Methods). Overall, encapsulation improved  $K_{\rm m}$ , maintained catalytic activity and efficiency at increasing lipid concentrations, and rescued the ribozymes from lipid-based inactivation.

# Single-turnover kinetics of hairpin ribozyme cleavage: the catalytic step is insensitive to lipids

The  $k_{\rm cat}$  determined from the multiple-turnover cleavage reactions encompasses several microscopic steps, including association, docking, cleavage, undocking, and product dissociation<sup>34</sup> (Figure 1B). To probe how lipids and encapsulation affect docking and cleavage independent of substrate association and product dissociation, we performed single-turnover cleavage reactions with the hairpin ribozyme and substrate RNA 1 and assayed them by gel electrophoresis, with a 10-fold excess of ribozyme over substrate (Figures 3A, S4G, S4H, and S4J). In the single-turnover case, the observed rate constant,  $k_{\text{obs,cleav}}$ , reflects the docking and cleavage steps, of which docking may be rate limiting.<sup>34</sup> The findings (STAR Methods) mirror the trends observed with  $k_{\rm cat}$  in the multiple-turnover condition. Thus, the presence of empty vesicles perturbs the catalytic steps somewhat, but the main inactivating effect of empty vesicles, seen prominently in the multiple-turnover scenario, occurs



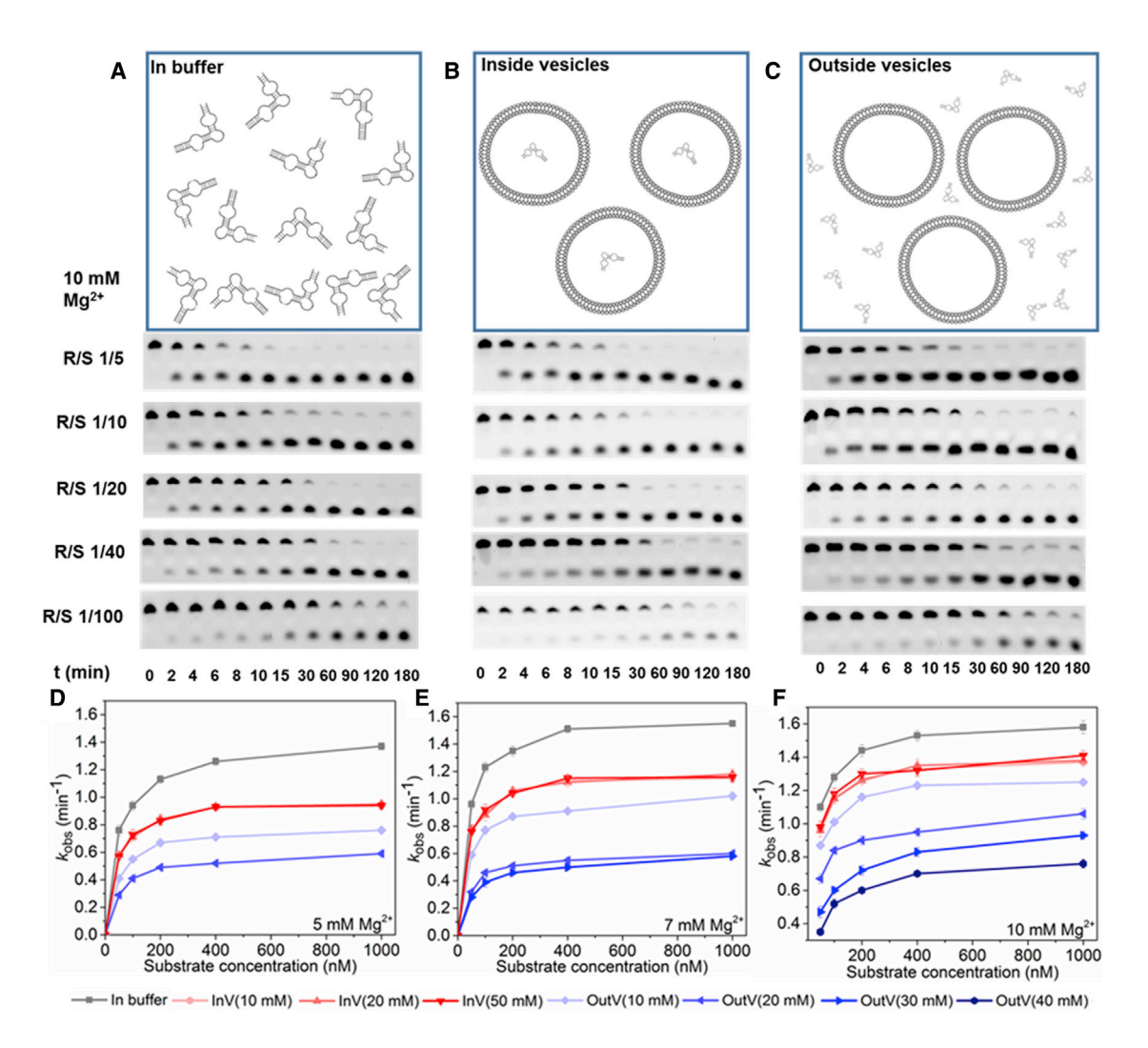


Figure 3. Gel assay following product formation from the hairpin ribozyme using substrate RNA and Michaelis-Menten plots of the hairpin ribozyme reaction

(A–C) Representative gels demonstrating the cleavage reaction at time intervals (t = 0, 2, 4, 6, 8, 10, 15, 30, 60, 90, 120, and 180 min) under different conditions: (A) in buffer, (B) encapsulated inside vesicles (InV), and (C) exposed to empty vesicles (OutV). In this experiment, [Mg<sup>2+</sup>] = 10 mM, and the ribozyme/substrate ratios (R/S) are 1/5, 1/10, 1/20, 1/40, and 1/100. The lipid concentration in the assays shown is 10 mM. See Figure 2A.

(D–F) Michaelis-Menten plots of the hairpin ribozyme reaction in the presence of excess substrate RNA, with reaction rate  $k_{\text{obs}}$  versus [substrate], for 5 mM (D), 7 mM (E), or 10 mM (F) Mg<sup>2+</sup>. Conditions were in lipid-free buffer (gray), encapsulated in vesicles (red, with [lipid] as indicated), or outside vesicles (blue, with [lipid] as indicated). Standard deviations from at least 3 replicates are shown by error bars. See also Figures 2A and S1–S3 and Tables S5 and S6.

primarily at non-catalytic steps (e.g., substrate association and dissociation).

# Encapsulation promotes docking of the hairpin ribozyme

Since confinement in a small volume is expected to stabilize compact structures relative to unfolded structures,  $^{15,29}$  we hypothesized that encapsulation may cause the observed effects on  $k_{\rm cat}$  of the hairpin ribozyme through stabilization of the docked conformation, which contains an essential tertiary contact on the reaction pathway. Formation of the docked conformation was measured using FRET (Figure 2B) in the following conditions: in the absence of vesicles, exposed to empty vesicles (OutV), or InV. The ribozyme was labeled with donor and

acceptor dyes and incubated with a non-cleavable modified RNA **5** as substrate (Figures S5A–S5D; Table S1). For the wild-type hairpin ribozyme (RNA **2**; Table S1), the largest FRET signal was observed in the absence of vesicles, consistent with the observation that  $k_{\rm cat}$  is also highest under this condition (Figure 5B and S5E–S5K; Table S2). Exposure of the ribozyme to empty vesicles reduced both the rate of docking and the overall FRET signal, indicating less docking as the amount of lipid increased, down to 44% signal and 38% rate (at 30 mM lipid) compared to the lipid-free solution. However, when the ribozyme was InV at the same lipid concentrations, the FRET signal equilibrated at ~79%, with the docking rate at ~70%, compared to the lipid-free solution. This indicates a shift toward the docked state when the ribozyme is encapsulated



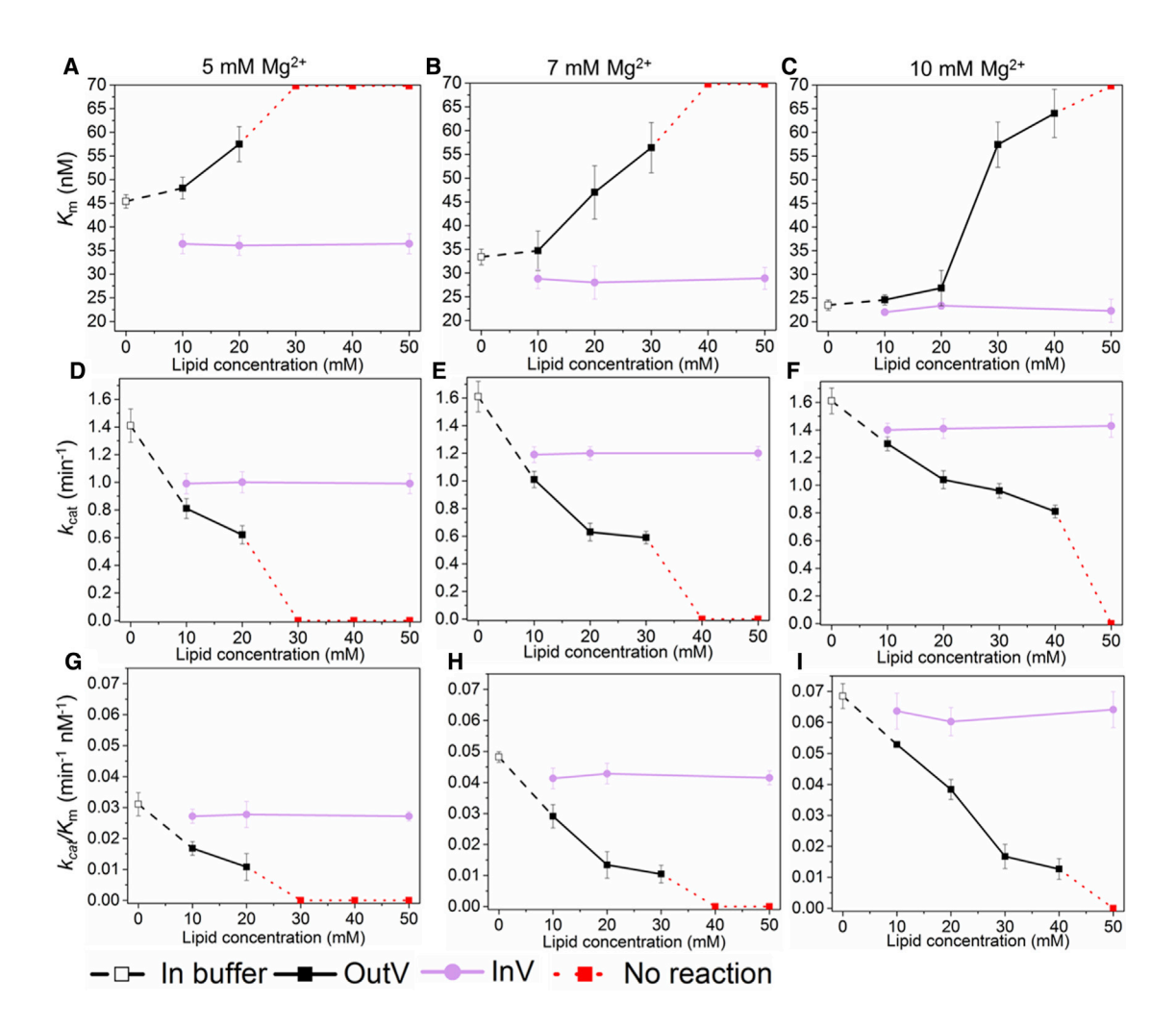


Figure 4. Dependence of  $K_{\rm m}$  (A–C),  $k_{\rm cat}$  (D–F), and  $k_{\rm cat}$ / $K_{\rm m}$  (G–I) of the hairpin ribozyme cleavage reaction on lipid concentration, in the presence of 5, 7, or 10 mM Mg<sup>2+</sup> (left, center, and right columns, respectively), under multiple-turnover conditions. The ribozyme and substrate RNA are either in buffer without lipids (black open squares; lipid concentration = 0), exposed to empty vesicles (OutV, black squares), or encapsulated inside vesicles (InV, purple circles). Red markers and dotted lines at the top (for  $K_{\rm m}$ ) or bottom (for  $k_{\rm cat}$  and  $k_{\rm cat}/K_{\rm m}$ ) of the horizontal axes indicate reactions for which no product was detected (Figure S4I). Each point is an average of 3 replicates, with error bars showing standard deviations.

See also Figures 2A and S1-S4 and Tables S5 and S6.

compared to the OutV condition. Furthermore, the FRET signal was insensitive to increasing lipid concentration when the ribozyme was encapsulated, in contrast to the OutV condition, in which the FRET signal and docking rate decreased as the [lipid] increased. The shift toward the docked state and the insensitivity of the FRET signal to [lipid] mirror the trends seen with cleavage activity of the ribozyme, supporting the idea that encapsulation promotes activity by favoring a compact tertiary conformation along the reaction pathway.

# Rescue of docking in folding-deficient ribozyme mutants via encapsulation

Since encapsulation was observed to favor the docked state, we tested whether encapsulation could rescue known folding-deficient mutants (C25U and A10G, 36,37 corresponding to RNA 3 and 4, respectively; Figures S5A-S5D; Table S1). These mutants normally exhibit no detectable docking in solution. The ribozymes were annealed with non-cleavable substrate RNA 5 to study docking by FRET. These mutants do not show detectable FRET signals in the absence of vesicles or when exposed to empty vesicles (Figures 5C and S5L-S5Z8). However, encapsulation of these mutants results in significant FRET signals, with mutant C25U recovering to ~36% and mutant A10G recovering to  $\sim 53\%$  of the wild-type docking signal amplitude (and to ~23% and 33%, respectively, for docking rate) (Table S2). In the case of mutant C25U, activity is known to be partly rescued by compensatory mutation G+1A in the substrate.<sup>36</sup> When mutant C25U was assayed with the compensatory substrate (RNA 6, Figures S5A-S5D; Table S1), docking was still not detectable in buffer (without lipids) or when exposed to empty vesicles (Figures S5Z2-S5Z8). However, encapsulation of the C25U/G+1A complex does result in higher FRET signals than those observed with C25U and substrate 5 (recovering to  $\sim$ 56% of both wild-type signal amplitude and docking rate),



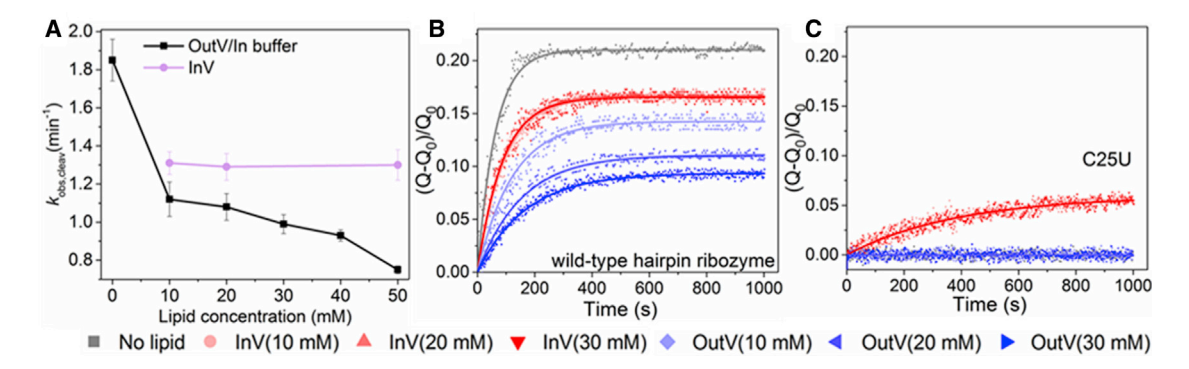


Figure 5. Dependence of the single-turnover hairpin ribozyme cleavage reaction (kobs,cleav) on lipid concentration and FRET study of mutants (A) Reactions were conducted with a ribozyme:substrate ratio of 10:1 and in the presence of 5 mM Mg<sup>2+</sup>. The ribozyme and substrate RNA are either in buffer without lipids (black square; lipid concentration = 0), OutV (black squares with lines), or encapsulated InV (purple circles with lines). Each point is an average of 3 replicates, with error bars showing standard deviations. See Figure 2A.

(B and C) Ribozyme docking measured by FRET for the hairpin ribozyme in lipid-free solution (gray), OutV (blue; lipid concentration indicated), or encapsulated InV (red; lipid concentration indicated). Docking of the wild type (B) and the mutant C25U (C) are shown with substrate RNA 5. Note that all of the conditions were tested in (C), and the lipid-free condition and all OutV conditions showed baseline FRET during the experiment. Relative FRET efficiency was calculated as a normalized ratio of acceptor:donor fluorescence ([Q], i.e.,  $[Q-Q_0]/Q_0$ , where  $Q_0$  is the initial value of Q). The docking rate was determined by nonlinear leastsquares fitting to the equation  $Q = Q_A (1 - e^{-kdockat})$ , where  $Q_A$  is the amplitude of the signal and  $k_{dock}$  is the rate constant. See also Figures 2, S4, and S5 and Table S2.

consistent with the known effect of G+1A. For encapsulated reactions, the level of FRET signal was insensitive to the lipid concentration, which is consistent with the earlier observations of kinetics. These results indicate that encapsulation restores and improves docking for these mutants.

# Cleavage activity of the mutants with vesicles

Given the improvements in docking observed for encapsulation. we then measured the catalytic activities of the folding-deficient mutants in the lipid-free buffer, encapsulated InV, or exposed to empty vesicles (OutV). These mutants are known to be capable of cleavage despite their folding defects. 36,37 Both mutants and the C25U/G+1A complex (using substrate RNA 7) showed higher cleavage activity when encapsulated InV compared to lipid-free buffer or OutV (Figures 6A-6C and S6A-S6C), with the observed rates being approximately doubled when encapsulated InV compared to lipid-free buffer (Table S3, Section 1). This observation indicates that the restoration of docking by encapsulation, as measured by FRET, corresponded to greater cleavage activity. Encapsulation increased cleavage activity over a lipid-free solution, indicating an advantage beyond overcoming the denaturing effect of lipids. As with the wild type, the beneficial effects of encapsulation were weaker in larger vesicles that had been extruded through 200-nm pores (Figures S6G-S6K; Table S3, Section 3).

# Ligation activity of folding-deficient mutants with vesicles

In the known folding pathway of the hairpin ribozyme, cleavage or ligation can occur only from the docked state.<sup>34</sup> For the cleavage reaction, the cleavage step can take place, and the fragments can dissociate upon undocking, even if the ribozyme is only transiently docked (undetectable by FRET). However, ligation is apparently more demanding, requiring a kinetically stable tertiary structure.<sup>37</sup> The folding-deficient mutants normally show no detectable ligation activity, and thus, ligation represents a stronger test of activity compared to cleavage. We studied the ligation activity of mutants A10G and C25U/G+1A in comparison to the wild-type hairpin ribozyme in lipid-free solution as well as the InV and OutV conditions. The reaction (Figure 2C) was monitored by gel electrophoresis using fluorescent substrate RNA 9 (wild type or A10G) or 10 (C25U/G+1A). As expected, the wildtype ribozyme showed ligation activity in all conditions (Figures 6D and S6D-S6F; Table S4, Section 1). As observed with the cleavage reaction, ligation activity decreased with increasing lipid concentration when the wild-type ribozyme was exposed to empty vesicles OutV, and encapsulation InV resulted in improved activity that was not affected by the lipid concentration.

Consistent with the FRET studies, the folding-deficient mutants showed no ligation activity in the absence of vesicles and also no activity when exposed to empty vesicles OutV. However, ligation activity was restored by encapsulation InV, consistent with the observation of restored docking in the FRET study. The C25U/G+1A complex was more active in the ligation reaction than the mutant A10G, consistent with the faster docking of C25U/G+1A, as indicated by the FRET study. The detection of ligation activity of the mutants confirmed that encapsulation substantially stabilized the docked conformation, to the extent that ligation was detectable. As seen for the cleavage reaction, the encapsulation effect for ligation was weaker in larger vesicles that had been extruded through 200 nm pores (Figures S6G-S6K; Table S4, Section 2).

# **Encapsulation of an RNA stem-loop structure**

Studies with the hairpin ribozyme suggested that encapsulation may affect both secondary (e.g., demonstrated by decreased  $K_{\rm m}$ ) and tertiary structure formation (e.g., docking). To directly test the effect of encapsulation on secondary structure formation alone, we studied the melting point of a stem-loop RNA (RNA 11; Table S1).47 The formation of the secondary structure was followed by FRET (Figure 7A). Exposure to vesicles destabilized



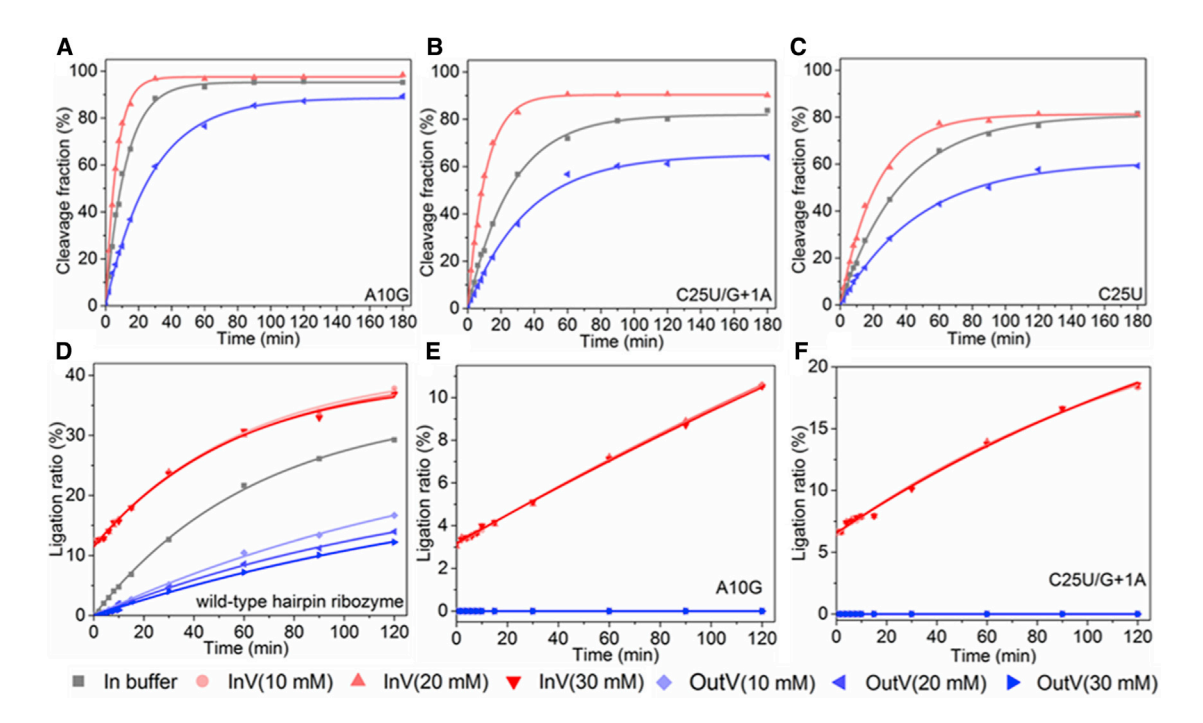


Figure 6. Cleavage and ligation activity of folding-deficient hairpin ribozyme mutants

(A–C) Kinetics of the multiple-turnover cleavage reaction ([ribozyme mutant]/[substrate] ratio = 1:20) in the presence of 5 mM Mg<sup>2+</sup> for the 3 folding-deficient mutants: (A) A10G, (B) C25U (with substrate G+1A), and (C) C25U. The lipid concentration of the vesicles is 20 mM for cleavage reactions in the InV and OutV conditions. See Figure 2A.

(D–F) Kinetics of the ligation reaction with ribozyme:substrate ratio of 1:1 in the presence of 10 mM Mg<sup>2+</sup>, for the wild-type hairpin ribozyme (D), mutant A10G (E), and C25U (substrate G+1A) (F). For reactions with lipids, the concentrations of the vesicles were 10, 20, or 30 mM, as indicated in the legend. In (E) and (F), the gray line for reaction in lipid-free buffer is present at approximately baseline throughout the experiment. Note that some ligation is present at time zero for the encapsulated reaction (D–F), as some ligation occurred during incubation at the lower [Mg<sup>2+</sup>] used to prepare the ligation-competent ribozyme (Figure 2C; STAR Methods). Solid lines are curve fits to a single exponential equation (see Table S4, Section 1).

See also Figures 2 and S6 and Tables S3 and S4.

the stem-loop structure, with the melting temperature  $T_{\rm m}$  being decreased by  $\sim$ 1.1°C, 4.4°C, and 5°C at lipid concentrations of 10, 20, and 30 mM, respectively (Figures 7B and S7A–S7G; Table S4, Section 3). However, the  $T_{\rm m}$  increased by  $\sim$ 2°C when the stem-loop RNA was encapsulated InV. The results indicate that encapsulation can stabilize base-pairing interactions between strands of nucleic acids.

# **Encapsulation of a DNA switch**

To test the generality of the observed promotion of tertiary contacts, we studied the folding of a pH-sensitive DNA switch. In this switch, a DNA triplex is formed at low pH, and high pH triggers the release of a single-stranded region from a duplex.<sup>48</sup> The release of the single-stranded DNA could be used to activate downstream events. 49,50 Here, the DNA was labeled with a fluorophore and quencher, such that the fluorescence is quenched when the triplex structure is formed, and fluorescence is recovered when the single-stranded region is released. The switch is characterized by its  $pK_a$ , which can be determined as the inflection point of the fluorescence curve over a pH range. In lipid-free solution, the p $K_a$  was observed to be 8.69  $\pm$  0.16. Consistent with our general observation that exposure to vesicles destabilizes folding, we found that exposure to empty vesicles destabilized the triplex relative to the duplex (Figures 7C, 7D and S7H-S7L), lowering the p $K_a$  by  $\sim$ 0.5 pH units, to 8.27  $\pm$  0.16 (10 mM lipid) or 8.11  $\pm$  0.15 (20 mM lipid). However, encapsulation inside vesicles stabilized the triplex beyond the p $K_a$  of the switch in lipid-free solution, raising the p $K_a$  by  $\sim\!1.0$  pH units (or by  $\sim\!1.5$  pH units compared to the switch exposed to empty vesicles), to 9.67  $\pm$  0.17 (10 mM lipid), or 9.68  $\pm$  0.13 (20 mM lipid). Thus, encapsulation significantly shifted the equilibrium of the DNA switch toward triplex formation, consistent with favoring the compacted structure.

# **DISCUSSION**

Prior studies indicated that encapsulation could increase aptamer and ribozyme activity, but the structural basis of this effect was unknown. <sup>15,16</sup> Here, we determined several effects of encapsulation on RNA and DNA structure and function. First, encapsulation can stabilize RNA structures. This was observed by FRET in the case of the hairpin ribozyme, in which encapsulation promoted docking and catalytic activity (STAR Methods). The possibility of encapsulation promoting RNA-RNA structures was further tested in an intramolecular context using an RNA sequence designed to fold into a stem-loop structure. The stem-loop RNA exhibited a higher melting temperature when encapsulated compared to both lipid-free solution and exposure to empty vesicles, indicating a stabilized secondary structure. This presents an interesting comparison with the

**Article** 



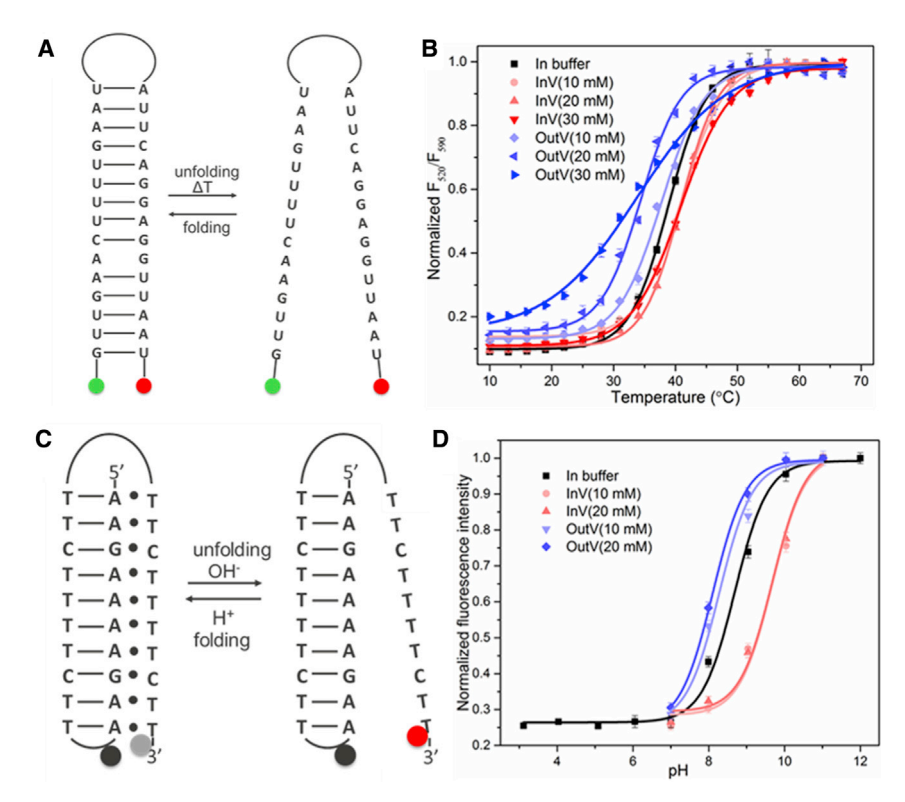


Figure 7. Effect of encapsulation on secondary structure formation of RNA and DNA (A and B) Melting of an RNA stem-loop structure monitored by FRET.

(A) Structure of the stem-loop RNA.

(B) The FRET-based melting curves of the stemloop RNA (ratio of donor emission fluorescence  $[\lambda=520~\text{nm}]$  to acceptor emission fluorescence  $[\lambda=590~\text{nm}]$ , normalized to 1), in the absence of vesicles (in buffer, black), InV (red), and OutV (blue). The lipid concentrations of the vesicles are 10, 20, or 30 mM, as indicated. Error bars indicate the standard deviations of 3 replicates (Table S4, Section 3). See Figures S7A–S7G for fluorescence spectra

(C and D) A triplex DNA switch is denatured to duplex structure by increasing pH, releasing fluorescence quenching.

(C) Structure of the triplex DNA switch.

(D) Fluorescence ( $\lambda_{ex} = 488$  nm,  $\lambda_{em} = 572$  nm) was measured at different pH, resulting in titration curves in the following conditions: in the absence of vesicles (black), InV (red), and OutV (blue). The lipid concentrations of the vesicles are 10 and 20 mM, as labeled. Three replicates were performed for each measurement.

See also Figure S7 and Table S4.

effects observed in the presence of molecular crowding agents<sup>21,24,51–58</sup> (STAR Methods) and indicates that both intramolecular and intermolecular RNA-RNA base-pairing associations were promoted by encapsulation.

A striking effect of encapsulation was the preservation of multiple-turnover catalytic activity of the hairpin ribozyme when subject to high concentrations of lipids that would otherwise inactivate the ribozyme. The presence of empty vesicles decreased  $k_{\rm cat}$ ,  $k_{\rm obs,cleav}$ , docking, and substrate association, leading to ribozyme inactivation in the multiple-turnover condition at high [lipid]. However, all of these steps mostly recovered when ribozymes were encapsulated. Encapsulation rendered the ribozymes essentially insensitive to lipid-based denaturation, as shown by the measurements of docking,  $K_{\rm m}$ ,  $k_{\rm cat}$ , and  $k_{\rm obs,cleav}$ . Thus, in addition to promoting secondary structures, encapsulation promoted a tertiary interaction along the reaction pathway, contributing to the observed preservation of catalytic activity under otherwise denaturing conditions (STAR Methods).

The ligation activity of the hairpin ribozyme represents a relatively stringent test of structure formation, particularly docking, since, in contrast to cleavage activity, the docked state must be substantially populated for ligation to occur. <sup>36,37</sup> This has been shown in particular for hairpin ribozyme constructs, in which the essential interdomain GC base pair (G+1C25) was replaced by either an AU pair or a GU wobble pair, as well as for a mutant in which the essential adenosine at position 10, involved in formation/stabilization of the active site, was replaced by a guanosine (A10G). These mutants still could cleave their respective substrates, but did not show detectable docking or ligation. <sup>36,37</sup> However, as shown here, encapsulation of these folding- and ligation deficient mutants restored both detectable docking and ligation

activity (see STAR Methods for a discussion of cleavage in the mutants). Encapsulation was shown to support activity of the hairpin ribozyme by strengthening important structural interactions. Similar effects have been observed through molecular crowding,  $^{18}$  in which the docking rate of the hairpin ribozyme (10 mM Mg $^{2+}$ , as used in the present FRET study) was observed to increase from 0% to 25% PEG-8000, up to a 7-fold increase in rate. In the present study, encapsulation increased the docking rate and amount by  $\sim\!1.8$ -fold compared to the OutV condition; a quantitatively similar increase was observed with  $\sim\!10\%$  PEG-8000 in the prior study. A similar effect was also observed for hairpin ribozymes under compression, wherein particular favorable interactions between the reaction site and neighboring nucleobases were suggested to be stabilized and to accelerate the cleavage step as a consequence.  $^{59}$ 

To test whether encapsulation would stabilize other tertiary interactions, we tested a pH-sensitive DNA switch, in which a triplex interaction forms at low pH and releases a single strand to adopt the duplex form at high pH. Considering the triplexduplex equilibrium as an acid-base reaction, encapsulation shifted the p $K_a$  of the triplex by  $\sim$ 1.0 pH units compared to DNA in lipid-free solution (or by  $\sim$ 1.5 pH units compared to the lipid-exposed DNA). This shift translates into a free energy stabilization of -1.4 kcal/mol compared to DNA in lipid-free solution (or −2.0 kcal/mol compared to lipid-exposed DNA). For context, these free energy stabilization values are similar in magnitude to the stabilization engendered by an additional base pair. 60 Interestingly, molecular crowders can also stabilize triplex formation, 61 consistent with the idea that vesicle confinement acts as an excluded volume effect. 15,29 The results showing a decreased effect in larger vesicles also supports the





interpretation that the confined volume causes the observed effects for the systems studied here. Encapsulation thus stabilized tertiary contacts in nucleic acids, as observed for both docking in the hairpin ribozyme and triplex formation in the DNA switch.

The observation that encapsulation stabilizes nucleic acid structures and rescues inactive mutants of the hairpin ribozyme has implications for the emergence and evolution of ribozymes in an RNA world. This stabilization would be particularly important in a prebiotic milieu containing a high concentration of lipids, which denature non-encapsulated RNA. The presence of lipids represents a double-edged sword for ribozymes: lipids increase the fitness of ribozymes that happen to become encapsulated, but they simultaneously depress, potentially severely, the fitness of ribozymes that are not encapsulated.

Given the general nature of the confinement effect in favoring compact (i.e., folded) structures for a variety of sequences, the frequency of sequences exhibiting an activity would increase if encapsulated, implying greater discoverability of such sequences from a random pool. In addition, as has been suggested for molecular crowding,<sup>26</sup> encapsulation would increase the mutational tolerance of a ribozyme. Tolerance to mutations would be a critical property, since replication error rates were likely high during the early stages of life. In particular, mutational tolerance would help avoid an "error catastrophe" by reducing the amount of information that must be replicated faithfully. 62,63 Furthermore, the stabilization of intermolecular RNA-RNA interactions may promote cooperative phenotypes, such as a system of mutually self-replicating ligases<sup>64</sup> or an autocatalytic set of recombinases,<sup>65</sup> or the formation of an active structure from smaller RNA subunits. 66-68 Thus, the physical confinement provided by encapsulation could facilitate the emergence of more complex catalytic activities during the origin of life.

# **STAR**\*METHODS

Detailed methods are provided in the online version of this paper and include the following:

- KEY RESOURCES TABLE
- RESOURCE AVAILABILITY
  - Lead contact
  - Materials availability
  - Data and code availability
- METHOD DETAILS
  - O Preparation of phospholipid/oleic acid vesicles
  - O Dynamic light scattering (DLS) measurement
  - Encapsulation of RNA or DNA
  - Cleavage experiments
  - Ligation experiments
  - O Fluorescence resonance energy transfer (FRET) measurement
  - Melting transitions of RNA measured by FRET
  - pH-titration measurements
  - Synthesis and labeling of RNAs
  - O Preparation of hairpin ribozymes by in vitro transcrip-
  - O Detailed kinetic analysis
  - DNA primer information

- Triplex DNA switch
- Comparison with crowding agents
- Lipid-based inactivation
- QUANTIFICATION AND STATISTICAL ANALYSIS

## SUPPLEMENTAL INFORMATION

Supplemental information can be found online at https://doi.org/10.1016/j. cub.2021.10.047.

## **ACKNOWLEDGMENTS**

The authors thank James Carothers and Matthew Lakin for advice regarding the DNA switch, Ranajay Saha for advice on encapsulation, and Ulrich Gerland for discussions about energetics. Funding from the Simons Foundation Collaboration on the Origin of Life (grant 290356FY18), the National Science Foundation (grant1935087), the National Institute of General Medical Sciences (grant DP2GM123457), the Camille Dreyfus Teacher-Scholar Program, and Deutsche Forschungsgemeinschaft (DFG\_MU1396/19) is acknowledged.

# **AUTHOR CONTRIBUTIONS**

H.P., S.M., and I.A.C. conceived and designed the study. H.P., A.L., and K.L. conducted the experimental work. H.P., S.M., and I.A.C. analyzed the data and drafted the manuscript. All of the authors commented on the manuscript.

# **DECLARATION OF INTERESTS**

The authors declare no competing interests.

Received: July 8, 2021 Revised: September 2, 2021 Accepted: October 21, 2021 Published: November 10, 2021

# **REFERENCES**

- 1. Pressman, A., Blanco, C., and Chen, I.A. (2015). The RNA World as a Model System to Study the Origin of Life. Curr. Biol. 25, R953-R963.
- 2. Saha, R., Pohorille, A., and Chen, I.A. (2014). Molecular crowding and early evolution. Orig. Life Evol. Biosph. 44, 319-324.
- 3. Ichihashi, N., and Yomo, T. (2014). Positive roles of compartmentalization in internal reactions. Curr. Opin. Chem. Biol. 22, 12-17.
- 4. Koonin, E.V. (2012). "RNA Worlds: From Life's Origins to Diversity in Gene Regulation" [book review]. Q. Rev. Biol. 87, 66.
- 5. Szostak, J.W., Bartel, D.P., and Luisi, P.L. (2001). Synthesizing life. Nature 409, 387-390.
- 6. Bansho, Y., Furubayashi, T., Ichihashi, N., and Yomo, T. (2016). Hostparasite oscillation dynamics and evolution in a compartmentalized RNA replication system. Proc. Natl. Acad. Sci. USA 113, 4045-4050.
- 7. Sunami, T., Ichihashi, N., Nishikawa, T., Kazuta, Y., and Yomo, T. (2016). Effect of Liposome Size on Internal RNA Replication Coupled with Replicase Translation. ChemBioChem 17, 1282-1289.
- 8. Hilburger, C.E., Jacobs, M.L., Lewis, K.R., Peruzzi, J.A., and Kamat, N.P. (2019). Controlling Secretion in Artificial Cells with a Membrane AND Gate. ACS Synth. Biol. 8, 1224-1230.
- 9. Zhang, Y., Chen, Y., Yang, X., He, X., Li, M., Liu, S., Wang, K., Liu, J., and Mann, S. (2021). Giant Coacervate Vesicles As an Integrated Approach to Cytomimetic Modeling. J. Am. Chem. Soc. 143, 2866-2874.
- 10. Dewey, D.C., Strulson, C.A., Cacace, D.N., Bevilacqua, P.C., and Keating, C.D. (2014). Bioreactor droplets from liposome-stabilized all-aqueous emulsions. Nat. Commun. 5, 4670.
- 11. Lentini, R., Santero, S.P., Chizzolini, F., Cecchi, D., Fontana, J., Marchioretto, M., Del Bianco, C., Terrell, J.L., Spencer, A.C., Martini, L.,

# **Article**



- et al. (2014). Integrating artificial with natural cells to translate chemical messages that direct E. coli behaviour. Nat. Commun. 5, 4012.
- Chen, I.A., Roberts, R.W., and Szostak, J.W. (2004). The emergence of competition between model protocells. Science 305, 1474–1476.
- Engelhart, A.E., Adamala, K.P., and Szostak, J.W. (2016). A simple physical mechanism enables homeostasis in primitive cells. Nat. Chem. 8, 448–453
- Black, R.A., Blosser, M.C., Stottrup, B.L., Tavakley, R., Deamer, D.W., and Keller, S.L. (2013). Nucleobases bind to and stabilize aggregates of a prebiotic amphiphile, providing a viable mechanism for the emergence of protocells. Proc. Natl. Acad. Sci. USA 110, 13272–13276.
- Saha, R., Verbanic, S., and Chen, I.A. (2018). Lipid vesicles chaperone an encapsulated RNA aptamer. Nat. Commun. 9, 2313.
- Lai, Y.-C., Liu, Z., and Chen, I.A. (2021). Encapsulation of ribozymes inside model protocells leads to faster evolutionary adaptation. Proc. Natl. Acad. Sci. USA 118, e2025054118.
- Doudna, J.A., and Cech, T.R. (2002). The chemical repertoire of natural ribozymes. Nature 418, 222–228.
- Paudel, B.P., and Rueda, D. (2014). Molecular crowding accelerates ribozyme docking and catalysis. J. Am. Chem. Soc. 136, 16700–16703.
- Strulson, C.A., Yennawar, N.H., Rambo, R.P., and Bevilacqua, P.C. (2013).
   Molecular crowding favors reactivity of a human ribozyme under physiological ionic conditions. Biochemistry 52, 8187–8197.
- Karimata, H., Nakano, S., and Sugimoto, N. (2006). The roles of cosolutes on the hammerhead ribozyme activity. Nucleic Acids Symp Ser (Oxf) 50, 81–82
- Nakano, S., Karimata, H.T., Kitagawa, Y., and Sugimoto, N. (2009). Facilitation of RNA enzyme activity in the molecular crowding media of cosolutes. J. Am. Chem. Soc. 131, 16881–16888.
- Desai, R., Kilburn, D., Lee, H.-T., and Woodson, S.A. (2014). Increased ribozyme activity in crowded solutions. J. Biol. Chem. 289, 2972–2977.
- Paudel, B.P., Fiorini, E., Börner, R., Sigel, R.K.O., and Rueda, D.S. (2018).
   Optimal molecular crowding accelerates group II intron folding and maximizes catalysis. Proc. Natl. Acad. Sci. USA 115, 11917–11922.
- Kilburn, D., Roh, J.H., Guo, L., Briber, R.M., and Woodson, S.A. (2010).
   Molecular crowding stabilizes folded RNA structure by the excluded volume effect. J. Am. Chem. Soc. 132, 8690–8696.
- Kilburn, D., Roh, J.H., Behrouzi, R., Briber, R.M., and Woodson, S.A. (2013). Crowders perturb the entropy of RNA energy landscapes to favor folding. J. Am. Chem. Soc. 135, 10055–10063.
- Lee, H.-T., Kilburn, D., Behrouzi, R., Briber, R.M., and Woodson, S.A. (2015). Molecular crowding overcomes the destabilizing effects of mutations in a bacterial ribozyme. Nucleic Acids Res. 43, 1170–1176.
- Rahman, M.S., Gulshan, M.A., Matsumura, S., and Ikawa, Y. (2020).
   Polyethylene glycol molecular crowders enhance the catalytic ability of bimolecular bacterial RNase P ribozymes. Nucleosides Nucleotides Nucleic Acids 39, 715–729.
- Strulson, C.A., Molden, R.C., Keating, C.D., and Bevilacqua, P.C. (2012).
   RNA catalysis through compartmentalization. Nat. Chem. 4, 941–946.
- Zhou, H.-X., and Dill, K.A. (2001). Stabilization of proteins in confined spaces. Biochemistry 40, 11289–11293.
- Feldstein, P.A., Buzayan, J.M., and Bruening, G. (1989). Two sequences participating in the autolytic processing of satellite tobacco ringspot virus complementary RNA. Gene 82, 53–61.
- 31. Hampel, A., and Tritz, R. (1989). RNA catalytic properties of the minimum (-)sTRSV sequence. Biochemistry 28, 4929–4933.
- Wilson, T.J., Nahas, M., Araki, L., Harusawa, S., Ha, T., and Lilley, D.M.J. (2007). RNA folding and the origins of catalytic activity in the hairpin ribozyme. Blood Cells Mol. Dis. 38, 8–14.
- Murchie, A.I.H., Thomson, J.B., Walter, F., and Lilley, D.M.J. (1998).
   Folding of the hairpin ribozyme in its natural conformation achieves close physical proximity of the loops. Mol. Cell 1, 873–881.

- Zhuang, X., Kim, H., Pereira, M.J.B., Babcock, H.P., Walter, N.G., and Chu, S. (2002). Correlating structural dynamics and function in single ribozyme molecules. Science 296, 1473–1476.
- van Tol, H., Buzayan, J.M., Feldstein, P.A., Eckstein, F., and Bruening, G. (1990). Two autolytic processing reactions of a satellite RNA proceed with inversion of configuration. Nucleic Acids Res. 18, 1971–1975.
- Pinard, R., Lambert, D., Walter, N.G., Heckman, J.E., Major, F., and Burke, J.M. (1999). Structural basis for the guanosine requirement of the hairpin ribozyme. Biochemistry 38, 16035–16039.
- Gaur, S., Heckman, J.E., and Burke, J.M. (2008). Mutational inhibition of ligation in the hairpin ribozyme: substitutions of conserved nucleobases A9 and A10 destabilize tertiary structure and selectively promote cleavage. RNA 14, 55–65.
- Liu, S., Bokinsky, G., Walter, N.G., and Zhuang, X. (2007). Dissecting the multistep reaction pathway of an RNA enzyme by single-molecule kinetic "fingerprinting.". Proc. Natl. Acad. Sci. USA 104, 12634–12639.
- Walter, N.G. (2001). Structural dynamics of catalytic RNA highlighted by fluorescence resonance energy transfer. Methods 25, 19–30.
- Hanczyc, M.M., Fujikawa, S.M., and Szostak, J.W. (2003). Experimental models of primitive cellular compartments: encapsulation, growth, and division. Science 302, 618–622.
- 41. Zhu, T.F., and Szostak, J.W. (2009). Coupled growth and division of model protocell membranes. J. Am. Chem. Soc. *131*, 5705–5713.
- Joyce, G.F., and Szostak, J.W. (2018). Protocells and RNA Self-Replication. Cold Spring Harb. Perspect. Biol. 10, a034801.
- Deamer, D.W., and Dworkin, J.P. (2005). Chemistry and physics of primitive membranes. In Prebiotic Chemistry, P. Walde, ed. (Springer), pp. 1–27.
- Jin, L., Kamat, N.P., Jena, S., and Szostak, J.W. (2018). Fatty Acid/ Phospholipid Blended Membranes: A Potential Intermediate State in Protocellular Evolution. Small 14, e1704077.
- Appel, B., Marschall, T., Strahl, A., and Müller, S. (2012). Kinetic characterization of hairpin ribozyme variants. In Ribozymes: Methods and Protocols, J.S. Hartig, ed. (Humana Press), pp. 41–59.
- Chen, I.A., Salehi-Ashtiani, K., and Szostak, J.W. (2005). RNA catalysis in model protocell vesicles. J. Am. Chem. Soc. 127, 13213–13219.
- 47. Gao, M., Arns, L., and Winter, R. (2017). Modulation of the Thermodynamic Signatures of an RNA Thermometer by Osmolytes and Salts. Angew. Chem. Int. Ed. Engl. 56, 2302–2306.
- Idili, A., Vallée-Bélisle, A., and Ricci, F. (2014). Programmable pH-triggered DNA nanoswitches. J. Am. Chem. Soc. 136, 5836–5839.
- Ashton, N.W., Bolderson, E., Cubeddu, L., O'Byrne, K.J., and Richard, D.J. (2013). Human single-stranded DNA binding proteins are essential for maintaining genomic stability. BMC Mol. Biol. 14, 9.
- Maffeo, C., and Aksimentiev, A. (2017). Molecular mechanism of DNA association with single-stranded DNA binding protein. Nucleic Acids Res. 45, 12125–12139.
- Gao, M., Gnutt, D., Orban, A., Appel, B., Righetti, F., Winter, R., Narberhaus, F., Müller, S., and Ebbinghaus, S. (2016). RNA Hairpin Folding in the Crowded Cell. Angew. Chem. Int. Ed. Engl. 55, 3224–3228.
- Zimmerman, S.B., and Trach, S.O. (1988). Effects of macromolecular crowding on the association of E. coli ribosomal particles. Nucleic Acids Res. 16 (14A), 6309–6326.
- Dupuis, N.F., Holmstrom, E.D., and Nesbitt, D.J. (2014). Molecular-crowding effects on single-molecule RNA folding/unfolding thermodynamics and kinetics. Proc. Natl. Acad. Sci. USA 111, 8464–8469.
- Lambert, D., and Draper, D.E. (2007). Effects of osmolytes on RNA secondary and tertiary structure stabilities and RNA-Mg2+ interactions. J. Mol. Biol. 370, 993–1005.
- Nakano, S., Karimata, H., Ohmichi, T., Kawakami, J., and Sugimoto, N. (2004). The effect of molecular crowding with nucleotide length and cosolute structure on DNA duplex stability. J. Am. Chem. Soc. 126, 14330–14331.



- 56. Spink, C.H., and Chaires, J.B. (1999). Effects of hydration, ion release, and excluded volume on the melting of triplex and duplex DNA. Biochemistry
- 57. Nakano, S., Yamaguchi, D., Tateishi-Karimata, H., Miyoshi, D., and Sugimoto, N. (2012). Hydration changes upon DNA folding studied by osmotic stress experiments. Biophys. J. 102, 2808-2817.
- 58. Rozners, E., and Moulder, J. (2004). Hydration of short DNA, RNA and 2'-OMe oligonucleotides determined by osmotic stressing. Nucleic Acids Res. 32, 248-254.
- 59. Schuabb, C., Kumar, N., Pataraia, S., Marx, D., and Winter, R. (2017). Pressure modulates the self-cleavage step of the hairpin ribozyme. Nat. Commun. 8, 14661.
- 60. SantaLucia, J., Jr., and Hicks, D. (2004). The thermodynamics of DNA structural motifs. Annu. Rev. Biophys. Biomol. Struct. 33, 415-440.
- 61. Sugimoto, N. (2014). Noncanonical structures and their thermodynamics of DNA and RNA under molecular crowding: beyond the Watson-Crick double helix. In International Review of Cell and Molecular Biology, R. Hancock, and K.W. Jeon, eds. (Academic Press), pp. 205-273.
- 62. Eigen, M. (1971). Selforganization of matter and the evolution of biological macromolecules. Naturwissenschaften 58, 465-523.
- 63. Kun, A., Santos, M., and Szathmáry, E. (2005). Real ribozymes suggest a relaxed error threshold. Nat. Genet. 37, 1008-1011.
- 64. Lincoln, T.A., and Joyce, G.F. (2009). Self-sustained replication of an RNA enzyme. Science 323, 1229-1232.
- 65. Vaidya, N., Manapat, M.L., Chen, I.A., Xulvi-Brunet, R., Hayden, E.J., and Lehman, N. (2012). Spontaneous network formation among cooperative RNA replicators. Nature 491, 72-77.

- 66. Doudna, J.A., and Cech, T.R. (1995). Self-assembly of a group I intron active site from its component tertiary structural domains. RNA 1, 36-45.
- 67. Tjhung, K.F., Shokhirev, M.N., Horning, D.P., and Joyce, G.F. (2020). An RNA polymerase ribozyme that synthesizes its own ancestor. Proc. Natl. Acad. Sci. USA 117, 2906-2913.
- 68. Wachowius, F., and Holliger, P. (2019). Non-Enzymatic Assembly of a Minimized RNA Polymerase Ribozyme. ChemSystemsChem 1, 1-4.
- 69. Fujikawa, S.M., Chen, I.A., and Szostak, J.W. (2005). Shrink-wrap vesicles. Langmuir 21, 12124-12129.
- 70. Östling, S., and Virtama, P. (1946). A Modified Preparation of the Universal Buffer Described by Teorell and Stenhagen. Acta Physiol. Scand. 11, 289-293.
- 71. Rublack, N., Nguyen, H., Appel, B., Springstubbe, D., Strohbach, D., and Müller, S. (2011). Synthesis of specifically modified oligonucleotides for application in structural and functional analysis of RNA. J. Nucleic Acids 2011, 805253.
- 72. Hegg, L.A., and Fedor, M.J. (1995). Kinetics and thermodynamics of intermolecular catalysis by hairpin ribozymes. Biochemistry 34, 15813-15828.
- 73. Nesbitt, S.M., Erlacher, H.A., and Fedor, M.J. (1999). The internal equilibrium of the hairpin ribozyme: temperature, ion and pH effects. J. Mol. Biol.
- 74. Donahue, C.P., Yadava, R.S., Nesbitt, S.M., and Fedor, M.J. (2000). The kinetic mechanism of the hairpin ribozyme in vivo: influence of RNA helix stability on intracellular cleavage kinetics. J. Mol. Biol. 295, 693-707.
- 75. Nahas, M.K., Wilson, T.J., Hohng, S., Jarvie, K., Lilley, D.M.J., and Ha, T. (2004). Observation of internal cleavage and ligation reactions of a ribozyme. Nat. Struct. Mol. Biol. 11, 1107-1113.

# **Current Biology Article**



# **STAR**\***METHODS**

# **KEY RESOURCES TABLE**

REAGENT or RESOURCE	SOURCE	IDENTIFIER
Chemicals, peptides, and recombinant proteins		
Phospholipid POPC	Avanti Polar Lipids	Catalog #: 850457C-25mg
Sepharose 4B	Millipore Sigma	Catalog #: 4B200-100ML
oleic acid	Millipore Sigma	Catalog #: O1008
nethanol	VWR	Catalog #: BDH1135-1LP
Klenow Fragment, exo-	Thermo Fisher	Catalog #: EP0421
DNase I	Thermo Fisher Scientific	Catalog #: 18047019
riton X-100	Millipore Sigma	Catalog #: T8787-50ML
Deoxynucleotide (dNTP) Solution Mix	New England Biolabs	Catalog #: N0447S
Magnesium chloride	Millipore Sigma	Catalog #: M8266-100G
Jrea	Millipore Sigma	Catalog #: U5378-100G
Critical commercial assays		
liScribe T7 High Yield RNA Synthesis Kit	New England Biolabs	Catalog #: E2040S
ADIFAB Kits	FFA Sciences	Catalog #: ADI-1-200
Digonucleotides		
5'-(FAM)CUC ACA GUC CUC UUU-3'	This paper, order from IDT	N/A
'-(FAM)CUC ACA AUC CUC UUU-3'	This paper, order from IDT	N/A
JCA GGA GGU UAAU(Atto565)-3'	This paper, order from IDT	N/A
S'-TAA TAC GAC TCA CTA TAG GGA GAA AGA BAG AAG TGA ACC AGA GAA A-3'	This paper, order from IDT	N/A
5'-TAC CAG GTA ATA TAC CAC AAC GTG TGT TC TCT GGT TCA CTT CTC T-3'	This paper, order from IDT	N/A
S'-TAA TAC GAC TCA CTA TAG GGA GAA AGA GAG AAG TGA ACC AGA GAA A-3'	This paper, order from IDT	N/A
5'-TAC CAG GTA ATA TAC CAC AAC GTG TAT TC TCT GGT TCA CTT CTC T-3'	This paper, order from IDT	N/A
5'-TAA TAC GAC TCA CTA TAG GGA GAA AGA GAG AGG TGA ACC AGA GAA A-3'	This paper, order from IDT	N/A
5'-TAC CAG GTA ATA TAC CAC AAC GTG TGT TC TCT GGT TCA CTT CTC T-3'	This paper, order from IDT	N/A
5'-AAGAA-AAGAA-TTT(BHQ-2)A-TTCTT-TTCTT- CTTTG-TTCTT-TTCTT(AF546)-3'	This paper, order from IDT	N/A
Software and algorithms		
OriginPro 2015	OriginLab Corporation	https://www.originlab.com/2015
ChemDraw Professional 18.0	PerkinElmer	https://www.perkinelmerinformatics.com/ products/research/chemdraw/
Other		
ECAN infinite 200 Pro plate reader	TECAN	https://lifesciences.tecan.com/plate_readers/infinite_200_pro
Amersham Typhoon RGB	GE Healthcare	http://www.cytivalifesciences.com/en/us/shop/ protein-analysis/molecular-imaging-for-proteins/ imaging-systems/amersham-typhoon-gel-and- blot-imaging-systems-p-00192
Fluoromax 4C	Horiba	https://www.horiba.com/en_en/products/detail/action/show/Product/fluoromax-1576/





# **RESOURCE AVAILABILITY**

# **Lead contact**

• Further information and requests for resources and reagents should be directed to and will be fulfilled by the lead contact, Irene Chen (ireneachen@ucla.edu).

# **Materials availability**

• This study did not generate new unique reagents.

# **Data and code availability**

- All data reported in this paper will be shared by the lead contact upon request.
- This paper does not report original code.
- Any additional information required to reanalyze the data reported in this paper is available from the lead contact upon request.

# **METHOD DETAILS**

# Preparation of phospholipid/oleic acid vesicles

The phospholipid/oleic acid vesicles were prepared according to previous methodology. <sup>69</sup> Briefly, 2.4 µL oleic acid in 200 µL methanol and 228 μL POPC in chloroform (25 mg/mL) were mixed well by vortexing and dried by rotary evaporation onto a round-bottom flask. One equivalent of 1 M KOH (7.6 µL) was added and the phospholipid/oleic acid solution was resuspended in 10 mM Tris-HCl (pH 7.5) buffer. The vesicles were prepared by extrusion through 100 nm (or 200 nm, when noted) polycarbonate membrane filters (Whatman) using a Mini-Extruder (Avanti Polar Lipids, Alabaster, AL). The vesicle solutions were concentrated by ultrafiltration to approximately 150 µL with an Amicon Ultra-4 10 000 filter. Assuming negligible loss of lipid, the lipid concentration after ultrafiltration is 100 mM (concentration of POPC + concentration of oleic acid). The concentration of oleic acid was verified by the ADIFAB assay (FFA Science, United States), 69 which measured 47 ± 3 mM fatty acid in the stock solution. Given the 1:1 ratio of oleic acid to phospholipid, the total measured lipid concentration in the stock was ~94 mM, which was comparable with the expected concentration of 100 mM.

# Dynamic light scattering (DLS) measurement

Vesicle size was measured by DLS using the Zetasizer Nano ZSP (Malvern Instruments, UK). Photons were collected at 173° scattering angle and the scattering intensity data were processed using the instrumental software to determine the hydrodynamic size of the vesicles.

# **Encapsulation of RNA or DNA**

The ribozyme and substrate RNA of designed ratios were mixed with buffer so as to obtain a final concentration of  $\sim$ 0.43-47  $\mu$ M RNA in 10 mM Tris-HCl (pH 7.5) buffer. This solution was added to the phospholipid/oleic acid micellar stock to prepare vesicles encapsulating RNA. For experiments on encapsulation of the ribozyme and substrate RNA inside vesicles, the unencapsulated RNA was removed by size exclusion chromatography (SEC) with Sepharose 4B resin (Figure S1B). Vesicles were extruded and purified from unencapsulated (free) RNAs using a Sepharose 4B size exclusion column (SEC) with a mobile phase of 10 mM Tris-HCl (pH 7.5) buffer. The vesicle solutions were concentrated by ultrafiltration to the desired lipid concentration (verified by ADIFAB assay as described above) with an Amicon Ultra-4 10 000 filter. The DNA switch and hairpin RNA structures were encapsulated in a similar way described above. The fluorescence signals of the collected products from SEC were measured on a TECAN infinite 200 Pro plate reader (TECAN, Switzerland).

# **Cleavage experiments**

For cleavage experiments without vesicles, the solution of the ribozyme and the 5'- fluorescein-labeled substrate strands (RNA 1 or 7) in 10 mM Tris-HCl (pH 7.5) were incubated at 90°C for 1 min followed by cooling to 37°C for 15 min. The cleavage reactions were started by adding an appropriate volume of the  $MgCl_2$  stock solution to the reaction mixture by brief pipetting at t = 0. In a typical cleavage experiment, final concentrations were 10 nM ribozyme, 50, 100, 200, 400 or 1000 nM (multiple turnover), or 1 nM (single turnover) substrate and 5 (7 or 10) mM MgCl<sub>2</sub> in a final volume of 20 μL. Aliquots (1.5 μL) of the reaction mixture were removed at time intervals and the reaction quenched by addition to 3 µL of stop mix (7 M urea, 50 mM EDTA). The samples were analyzed by 12% denaturing polyacrylamide gel electrophoresis and imaged using Amersham Typhoon Gel Imager (GE, USA). For cleavage experiments of RNA exposed to empty vesicles, the lipid concentrations were adjusted to 10, 20, 30, 40 and 50 mM. The aliquots of the reaction mixture were added to 3 μL of stop mix (7 M urea, 50 mM EDTA) with 0.6% Triton X-100 to rupture the vesicle for 30 min at

# **Current Biology Article**



room temperature. For experiments using non-extruded vesicles, vesicles were prepared in the same manner without the extrusion step, lipid concentrations were adjusted to match experiments with extruded vesicles, and cleavage experiments were performed as described above. For cleavage experiments of RNA encapsulated in vesicles, the lipid concentrations were 10, 20 and 50 mM. Vesicles were extruded to 100 nm unless otherwise noted, and experiments were performed following the same procedure regardless of vesicle extrusion size. At least three independent replicate datasets were collected.

# **Ligation experiments**

The wild-type hairpin ribozyme and mutants A10G and C25U/G+1A (see STAR Methods for sequences) were used for the ligation experiments. In general, ligation-competent ribozyme-substrate complex is prepared by annealing the ribozyme strand with a cleavage substrate and conducting the cleavage reaction. Dissociation of the smaller 3' cleavage product results in the ribozyme strand in complex with the 5' substrate strand. Then, addition of a fluorescently labeled 3' substrate strand and higher [Mg<sup>2+</sup>] allows assessment of ligation activity (Figure 2C). For ligation experiments without vesicles, 20  $\mu$ L of the ribozyme (200 nM) and the unlabeled substrate (100 nM; RNA 8) strands in 10 mM Tris-HCl (pH 7.5) were incubated at 90°C for 1 min followed by cooling to 37°C for 15 min. Then an appropriate volume of the MgCl<sub>2</sub> stock solution was added to the reaction mixture by brief pipetting for the final Mg<sup>2+</sup> concentration of 7 mM. The sample was incubated at 37°C for 1 h. Then the appropriate amount of 5'- fluorescein-labeled ligation substrate (RNA 9 or 10; see Table S1) stock solution and MgCl<sub>2</sub> stock solution were added to the reaction mixture to make the final ratio of ribozyme: ligation substrate equal to 1:1 and the Mg<sup>2+</sup> concentration equal to 10 mM; the time of this addition was defined as time t = 0. Aliquots (1.5  $\mu$ L) of the reaction mixture were removed after adding the ligation substrate, at particular time intervals, and the reaction quenched by addition to 8.5 μL of stop mix (7 M urea, 50 mM EDTA). The samples were analyzed by 12% denaturing polyacrylamide gel electrophoresis and imaged using an Amersham Typhoon Gel Imager (GE, USA).

For ligation experiments of RNA exposed to empty vesicles, the reaction procedure is identical to that mentioned above but with the lipid concentrations included in the buffer equal to 10, 20 or 30 mM. The aliquots of the reaction mixture were quenched by addition of 8.5 µL of stop mix (7 M urea, 50 mM EDTA) with 0.6% Triton X-100 and incubated for 30 min at room temperature to rupture the vesicles.

For ligation experiments of RNA encapsulated in vesicles, the fluorescently labeled ligation substrate could not be added during a second step. Instead, the ribozyme, cleavage substrate and fluorescently labeled ligation substrate were annealed together (incubated at 90°C for 1 min followed by cooling to 37°C for 15 min) and encapsulated in the vesicles as described above. The concentration of Mg<sup>2+</sup> was brought 7 mM and the reaction was incubated at 37°C for 1 h to prepare the ligation-competent ribozyme complex. The concentration of  $Mg^{2+}$  was then brought to 10 mM, defining t = 0. Aliquots (1.5  $\mu$ L) of the reaction mixture were removed at time intervals and the reaction quenched by addition to 8.5 µL of stop mix (7 M urea, 50 mM EDTA) with 0.6% Triton X-100 and incubation for 30 min at room temperature to rupture the vesicles. The lipid concentrations were the same as mentioned above for the reactions exposed to empty vesicles. At least three independent datasets were collected. Ligation experiments using vesicles of different sizes were performed in the same way.

# Fluorescence resonance energy transfer (FRET) measurement

The FRET measurement was performed on a Fluoromax 4C (Horiba) with a Peltier-controlled temperature attachment (Model F-3004, Horiba). The wild-type hairpin ribozyme (RNA 2), mutants A10G (RNA 4), C25U (RNA 3), and C25/G+1A (RNA 3 + 6), and the corresponding non-cleavable substrate (RNA 5 or 6) (Figures S5A-S5D; Table S1) were used for FRET measurements. Doubly labeled ribozyme (50 nM; see below for labeling method) and a 20-fold excess of non-cleavable substrate were mixed and pre-incubated in 10 mM Tris-HCl (pH 7.5) at 37°C for 15 min, before manually adding MgCl<sub>2</sub> stock solution (final concentration = 10 mM) to initiate domain docking. Atto 488 was excited at 450 nm. Fluorescence emission was monitored at both 520 nm (for the Atto 488 donor) and 590 nm (for the Atto 565 acceptor), and the ratio  $Q = F_{590}/F_{520}$  was calculated as a function of time. This ratio Q was normalized by its initial value  $Q_0$  (i.e.,  $y = (Q - Q_0)/Q_0$ ). The resulting curves were fitted with the exponential function  $y = A(1 - e^{-k \operatorname{dock} t})$ . Here  $k_{\operatorname{dock}}$  is the observed docking rate constant and A is the observed relative docking amplitude. For FRET measurement of RNA exposed to empty vesicles, vesicles with the desired lipid concentrations were mixed with the ribozyme and non-cleavable substrate strands and preincubated in 10 mM Tris-HCl (pH 7.5) at 37°C for 15 min before manually adding MgCl<sub>2</sub> stock solution. For FRET measurement of RNA encapsulated inside vesicles, the ribozyme and non-cleavable substrate were annealed together by heating to 90°C for 1 min, followed by cooling down to 37°C for 15 min before encapsulation as described above. Then, vesicles containing the ribozyme and non-cleavable substrate strands were preincubated in 10 mM Tris-HCl (pH 7.5) at 37°C for 15 min, before manually adding MgCl<sub>2</sub> stock solution to initiate docking.

# **Melting transitions of RNA measured by FRET**

A stock solution (100 μM) of the FRET-labeled stem-loop RNA 11 was heated to 75°C for 5 min and slowly cooled down to room temperature to anneal the RNA structure. The fluorescence of the dye-labeled RNA was measured at different temperatures using a Fluoromax 4C (Horiba) with a Peltier-controlled temperature attachment (Model F-3004, Horiba). The fluorescence of the labeled RNA was recorded in 3°C increments from 10 to 67°C, with a 10 min incubation at each interval. Fluorescence intensity spectra (excitation at 450 nm, and emission spectrum between 480 and 700 nm) were recorded. Melting curves were fitted in Origin Pro 9 software using the Boltzmann sigmoidal equation  $R = R_{min} + (R_{max} - R_{min})/(1 + \exp((T_t - T)/s))$ , where R refers to normalized fluorescence





intensity ratio of  $F_{520nm}/F_{590nm}$ , and  $R_{min}$  and  $R_{max}$  are the minimum and maximum values, respectively, T is temperature,  $T_t$  is the transition temperature, and s is a fitting parameter.  $T_t$  values presented here are an average of three independent experiments.

## pH-titration measurements

The pH-titration curves of the pH-sensitive DNA switch (100 nM; STAR Methods) were conducted in a universal citrate/phosphate/borate buffer whose pH was adjusted to the desired value. The solutions of the universal buffer at different pH were prepared according to a previously reported method. Equilibrium fluorescence measurements were obtained using a Fluoromax-4C spectrofluorometer (Horiba) with excitation at 488 nm and acquisition between 540 and 650 nm at 25°C. The normalized fluorescence data F (at 572 nm) was fitted with the following equation:  $F = F_0 + (F_m - F_0) \times 10^{-k}/(10^{-k} + 10^{-x})$ . In this equation,  $F_0$  is the minimum fluorescence signal (triplex state);  $F_m$  is the maximum fluorescence signal (duplex state);  $F_m$  is the pH of the inflection point, and  $F_m$  is the pH of the solution.

# Synthesis and labeling of RNAs

RNAs (Table S1) were chemically synthesized on a GeneAssembler (Pharmacia) using phenoxyacetyl (PAC) protected  $\beta$ -cyanoethyl-(N,Ndiisopropyl)-phosphoramidites of 5'-O-dimethoxytrityl-2'-O-tertbutyldimethylsilyl (TBDMS) nucleosides as described previously. RNA sequences A\_WT, A\_MUT C25U and A\_MUT A10G were modified at the 5'-terminus with an amino linker using C6-NH<sub>2</sub> phosphoramidite, and at the 3'-terminus with an alkynyl group using 2'-O-propargyluridine-3'-lcaa on CPG 1000 Å. RNAs Lig\_3'-Frag G and Lig\_3'-Frag A were modified at the 3'-terminus only with an alkynyl group. All RNAs were purified on 15% denaturing polyacrylamide gels, product-containing bands were cut from the gel, and RNAs were eluted (0.3 M NaOAc, pH 7.1) followed by ethanol precipitation.

Double labeling of A\_WT, A\_MUT C25U and A\_MUT A10G was performed with Atto488 NHS-ester and Atto565-azide (ATTO-TEC) in a one-pot reaction. Atto488 NHS-ester (150  $\mu$ g) was dissolved in 30  $\mu$ L dry DMF and added to the RNA (6 nmol) in 50  $\mu$ L sodium carbonate buffer (0.2 M, pH 8.5). The reaction was allowed to proceed under shaking for 4 h at 25°C. Subsequently, the Atto488-labeled RNA was added to 50  $\mu$ g dry Atto565-azide. A mixture of 50  $\mu$ L CuSO<sub>4</sub> (1mM in phosphate buffer 0.1 M, pH 7) and 50  $\mu$ L tris(3-hydroxypropyltriazolylmethyl) amine (5 mM in phosphate buffer 0.1 M, pH 7) was saturated with argon for 5 min and added to the RNA solution, which was again degassed with argon for 5 min. Thereafter, 65  $\mu$ L of freshly prepared sodium ascorbate solution (8 mM) was saturated with argon for 10 min and added to the reaction mixture. Finally, 240  $\mu$ L phosphate buffer (0.1  $\mu$ M, pH 7) were added to the solution. After incubation for 4 h at 37°C, the labeled RNA was precipitated from ethanol. 3′ end labeling of Lig\_3′-Frag G and Lig\_3′-Frag A with 5′-FAM (Jena Biosciences) was carried out according to the suppliers' protocol. All labeled RNAs were purified by RP-HPLC (EC 250/4 Nucleodur 100-5 C18, column volume (cv) = 3.142 mL) using buffer A (0.1 M TEAAc, 5% acetonitrile) and a gradient of buffer B (0.1 M TEAAc, 30% acetonitrile): 10% buffer B for 2 cv, 50% buffer B for 5 cv, 80% buffer B for 25 cv and 100% buffer B for 2 cv, at a flow rate of 0.5 mL/min. The isolated labeled RNAs were desalted by gel filtration and stored at -20°C until further use.

# Preparation of hairpin ribozymes by in vitro transcription

Hairpin ribozymes were enzymatically synthesized by *in vitro* transcription from a double-stranded DNA template. To generate the DNA template, a Klenow polymerase fill-in reaction was performed using two primers overlapping at their 3' ends (STAR Methods). Primers with a final concentration of 2  $\mu$ M in a reaction volume of 500  $\mu$ L were mixed with the Klenow buffer (50 mM Tris pH 7.6, 10 mM MgCl<sub>2</sub> and 50 mM NaCl) and heated for 2 min at 90°C. After incubation at 37°C for 15 min, the reaction was started by addition of dNTPs (0.5 mM) and the Klenow fragment exo— (final concentration 0.05 U  $\mu$ L<sup>-1</sup>). The reaction was carried out for 30 min at 37°C. The DNA was ethanol-precipitated and purified on a native polyacrylamide gel, eluted from the gel and desalted by ethanol precipitation. For *in vitro* transcription, DNA (1  $\mu$ M) in transcription buffer (80 mM HEPES pH 7.5, 22 mM MgCl<sub>2</sub>, 2 mM spermidine, 40 mM dithiothreitol) was mixed with 2  $\mu$ M NTPs, and 5  $\mu$ L of T7 RNA polymerase (1 U  $\mu$ L<sup>-1</sup>) was added to a final volume of 50  $\mu$ L. Transcription was performed for 2.5 h at 37°C. The DNA template was degraded by addition of DNase I (2 U) followed by incubation at 37°C for 30 min. RNA was recovered by ethanol precipitation, purified by 12% denaturing polyacrylamide gel electrophoresis, eluted from the gel and desalted by ethanol precipitation.

# **Detailed kinetic analysis**

For each condition, time-dependent data were fit to a single exponential equation to obtain observed rates ( $k_{obs}$ ) at each ribozyme:-substrate ratio (Figures S1 and S2), and the Michaelis-Menten constants ( $K_m$  and  $k_{cat}$ ) were determined by Eadie-Hofstee analysis. The cleavage reactions fit the Michaelis-Menten kinetic model well (Figures S3A-S3F). Rates increased with increasing substrate concentration until saturation, confirming the multiple-turnover nature of the reaction when encapsulated (Figures 3D-3F; Tables S5 and S6, Section 1).

Interestingly, in contrast to  $K_{\rm m}$ ,  $k_{\rm cat}$  for encapsulated ribozymes was lower than for the ribozyme in lipid-free solution (Figures 4D–4F). One interpretation of this finding is that the internal equilibrium of the hairpin ribozyme reaction may be shifted toward ligation (away from cleavage), <sup>38,72–75</sup> leading to reduction of  $k_{\rm cat}$  determined for the cleavage reaction. At the same time, ligation would be expected to become more pronounced (see results for ligation assay below). For  $k_{\rm cat}/K_{\rm m}$ , increased  $K_{\rm m}$  compensated for decreased  $k_{\rm cat}$ , such that  $k_{\rm cat}/K_{\rm m}$  of encapsulated ribozymes was similar to that in a lipid-free solution. Thus, encapsulation preserves catalytic activity and efficiency in the presence of otherwise denaturing lipids.

# Article



At medium (7 mM) and high (10 mM) [Mg<sup>2+</sup>], exposure to  $\geq$  40 mM or to 50 mM lipid, respectively, caused inactivation, but encapsulation again preserved ribozyme activity at the highest [lipid] tested (50 mM). To determine whether extrusion altered the effect of the lipid vesicles, we compared vesicles with or without extrusion (OutV condition). Ribozyme activity (5 mM Mg<sup>2+</sup>, 10 mM lipid) in both cases was similar (Figures S3G and S3H; Table S3, Section 2; compare to Figures 3D-3F), indicating that the denaturing effect of lipid exposure (OutV) was not very dependent on vesicle size and shape. To determine whether the confinement volume influenced the effect, we found that the beneficial effects of encapsulation were weaker in larger vesicles that had been extruded through 200 nm pores (Figures S4A-S4F; Table S6, Sections 2 and 3).

Single-turnover kinetics: As expected, comparison to  $k_{\text{cat}}$  (Figure 4D) showed that  $k_{\text{obs.cleav}} > k_{\text{cat}}$ , indicating that additional steps (undocking, dissociation and association) affect  $k_{cat}$  in the multiple-turnover reaction. In the single-turnover reactions at low [lipid], the presence of lipids (both InV and OutV conditions) caused a decrease in kobs, clear that was quantitatively similar to the drop observed for  $k_{\text{cat}}$  under the same Mg<sup>2+</sup> and lipid conditions. Interestingly, in contrast to the multiple-turnover reactions, high lipid concentrations did not completely inactivate the reaction in the OutV condition (compare Figure 5A to Figures 4A, 4D, and 4G). Nevertheless,  $k_{\text{obs.cleav}}$  decreased as [lipid] increased in the OutV condition, but not when encapsulated (InV). Similarly, the extent of reaction also dropped significantly as [lipid] increased for the OutV condition, but not the InV condition (Figure S4H).

For the wild-type and mutant ribozymes, exposure to lipids (OutV) causes a roughly two-fold decrease in  $k_{obs}$ . In the wild-type ribozyme, encapsulation causes only a small increase in  $k_{obs}$  compared to OutV, such that the encapsulated  $k_{obs}$  is lower than for the lipid-free environment. In contrast, for the mutants, encapsulation leads to relatively large effect on  $k_{obs}$ , such that the encapsulated  $k_{obs}$  is greater than that of the lipid-free environment. The wild-type ribozyme shows stable docking in buffer, and encapsulation was observed to have only a minor effect on an already stable docking process by FRET. This was reflected in the  $k_{obs}$  values, which are determined with  $k_{dock}$  or  $k_{undock}$  being the rate-limiting steps for the wild-type. The minor nature of the effect resulted in the overall finding that encapsulation did not fully compensate for the denaturation caused by exposure to the lipids (Figure 5A). So, in the wildtype ribozyme, the docked complex is only slightly affected by being inside the vesicle (as shown by the FRET data), and with docking/undocking rates being rate-limiting,  $k_{obs}$  shows only a minor effect.

With respect to the mutants, there is no stable docking observed in the lipid-free environment, and encapsulation causes a sufficiently large effect to observe a stably docked state. For the mutants, in particular for the A10G variant, higher cleavage rates than for the wild-type have been observed in vitro, 37 and it has been suggested that fast docking/undocking steps lead to a transiently docked complex, sufficient for cleavage to take place, such that docking/undocking steps are no longer rate-limiting. However, our FRET data shows that encapsulation leads to a detectable, stably docked complex, and therefore docking/undocking may be rate-limiting again. The large effect of encapsulation on docking is thus consistent with the observed relatively large increase in kobs, which results in the encapsulated  $k_{obs}$  being greater than the lipid-free  $k_{obs}$ .

Although the FRET constructs probe an effectively intramolecular interaction, while the cleavage experiments probe an intermolecular reaction, the size of the effect of encapsulation on docking can be compared to the size of effect on cleavage kinetics. In the FRET assay, encapsulation results in a  $\sim$ 1.8-fold increase in both docking rate and amount. Docking is expected to affect both  $K_m$ and k<sub>cat</sub>. In the multiple-turnover reaction performed at the same conditions as the FRET studies (10 mM Mg<sup>2+</sup>, 30 mM lipid), encapsulation causes the  $K_m$  to decrease by approximately 2.5-fold (comparing the InV and OutV conditions), and causes the  $k_{cat}$  to increase by ~1.4-fold (comparing InV and OutV). Although the FRET constructs and cleavage constructs are different, the similarity of the magnitudes of these effects suggests that encapsulation effects on docking may be sufficient to explain most of the effect on  $K_m$  and  $k_{cat}$  of the multiple-turnover reaction. Encapsulation might cause other effects as well, such as changes in effective concentration or alterations in  $pK_a$  of catalytically involved residues, but these do not appear necessary to explain the overall effect in this case. The difference in  $K_m$  between encapsulated ribozymes versus ribozymes in lipid-free solution decreased as Mg<sup>2+</sup> concentration increased, indicating that encapsulation could compensate for low  ${
m Mg}^{2+}$  with respect to  $K_{
m m}$ . However, changes in  $K_{
m m}$  could also reflect changes in  $k_{\text{cat}}$  ( $K_{\text{m}} = (k_{-1} + k_{\text{cat}})/k_1$ ).

# **DNA** primer information

The following primers were used to synthesize DNA templates for in vitro transcription preparing hairpin RNA ribozymes. The underlined sequences are overlapping, and the mutant bases are marked in bold.

# Wild-type hairpin ribozyme

Forward primer: 5'-TAA TAC GAC TCA CTA TAG GGA GAA AGA GAG AAG TGA ACC AGA GAA A-3' Reverse primer: 5'-TAC CAG GTA ATA TAC CAC AAC GTG TGT TTC TCT GGT TCA CTT CTC T-3'

# **Mutant C25U**

Forward primer: 5'-TAA TAC GAC TCA CTA TAG GGA GAA AGA GAG AAG TGA ACC AGA GAA A-3' Reverse primer: 5'-TAC CAG GTA ATA TAC CAC AAC GTG TAT TTC TCT GGT TCA CTT CTC T-3'

# **Mutant A10G**

Forward primer: 5'-TAA TAC GAC TCA CTA TAG GGA GAA AGA GAG AGG TGA ACC AGA GAA A-3' Reverse primer: 5'-TAC CAG GTA ATA TAC CAC AAC GTG TGT TTC TCT GGT TCA CTT CTC T-3'





# **Triplex DNA switch**

The triplex pH-triggered DNA switch is labeled with BHQ-2 (Black hole quencher 2) at position 13 and with Alexa Fluor 546 (AF546) at the 3'end (synthesized by IDT). The sequence of the DNA switch is the following:

5'-AAGAA-AAGAA-TTT(BHQ-2)A-TTCTT-TTCTT-CTTTG-TTCTT-TTCTT(AF546)-3'

# **Comparison with crowding agents**

In the case of an RNA stem-loop structure studied in the presence a variety of crowding agents,<sup>51</sup> addition of PEG resulted in increased T<sub>m</sub>, by up to 13.4°C, with the effect size depending on the PEG molecular weight. On the other hand, chemical interactions with the crowding agent can be significant as well; in one study, addition of ethylene glycol and low molecular weight PEG were found to decrease the  $T_m$  of DNA duplexes  $^{55}$  by up to  $16^{\circ}$ C, depending on the DNA length and PEG size. In the present study, encapsulation caused a  $2-7^{\circ}$ C increase in  $T_{\rm m}$  (depending on the lipid concentration of the OutV comparison), roughly equivalent to addition of 30% PEG-400 or PEG-6000 in the prior study<sup>51</sup> of an RNA stem-loop.

## **Lipid-based inactivation**

In this work, we demonstrated that vesicle encapsulation stabilizes both secondary and tertiary structure elements, as well as intermolecular base-pairing, and thus can impact the activity of functional nucleic acids. These studies also give insight into the phenomenon of lipid-based inactivation, namely that exposure to empty vesicles causes a decrease of activity, or at high concentrations, elimination of activity. This effect is due to exposure to vesicles, rather than to exposure to micelles or molecular lipid, since the denaturing effect increases at concentrations much higher than the critical aggregation concentration (cac) (i.e., upon addition of vesicles at constant micelle and molecular lipid concentration). The concentration of non-vesicular oleic acid (OA) in a 1:1 POPC/ OA system was measured to be 3.5 μM, an estimate of the cac<sup>44</sup>; lipid concentrations used in these experiments were several orders of magnitude larger than the cac. The encapsulation effect may be measured against the OutV condition in order to isolate the confinement effect, controlling for the effect of chemical exposure to the lipid. 15 The OutV condition may exclude a small fraction of volume (< 10% for up to 30 mM lipid; see Saha et al. 15 for calculation), but a possible excluded volume effect was apparently not large enough to counter the denaturing effect in these experiments.

# **QUANTIFICATION AND STATISTICAL ANALYSIS**

All statistics were performed in OriginPro 2015 (OriginLab). All values are shown as mean ± standard error of the mean (SEM), as specified in the corresponding figure and table legends.